# Complete optical spectrum of $CeAl_3$

A. M. Awasthi,* L. Degiorgi,† and G. Grüner
*Department of Physics and Solid State Science Center, University of California, Los Angeles, Los Angeles, California 90024*

Y. Dalichaouch and M. B. Maple
*Department of Physics, University of California, San Diego, San Diego, California 92093*
(Received 13 April 1993)

We report on optical conductivity measurements performed on $CeAl_3$ spanning the photon energy range between approximately zero and 12 eV. From the measurements at micrometer- and millimeter-wave frequencies we obtained the detailed temperature dependence of both components of the complex conductivity. These results as well as the Kramers-Kronig analysis performed on the absorptivity lead, at low temperatures, to a strongly frequency- and temperature-dependent dynamic conductivity. We analyze the optical conductivity in terms of frequency-dependent scattering rate and dynamical mass. The low-temperature effective mass is found to be $m^*/m_b = 325 \pm 50$ in the zero-frequency limit and its temperature dependence is compared with that of the thermodynamic parameters.

## I. INTRODUCTION

In the past decade, considerable theoretical[1–7] and experimental[8–12] effort has been devoted to the understanding of the electrodynamic response of correlated metals. Various theories suggest that the optical conductivity of the heavy-fermion (HF) ground state is characterized by a so-called renormalized Drude behavior at low frequencies. Also predicted is a minimum in $\sigma_1$ near $h\nu \sim k_B T_K$ ($2\pi\nu = \omega$), at the onset of a broad background at higher frequencies (Fig. 1). Here, $T_K$ denotes the Kondo temperature, the energy scale for many-body correlations in the heavy-fermion compound.[1] The broad feature at about $\Delta$ is usually identified with the excitations across the $s$-$f$ ($d$) hybridization gap.[3,7] Correspondingly, the real part of the dielectric function $\varepsilon_1(\omega)$ is expected to have two zero crossings (where $\varepsilon_1$ goes from negative to positive values with increasing frequency). The one at high frequency is identified with the plasma frequency ($\omega_p^2 = 4\pi n_c e^2/m_b$) of the uncorrelated conduction electrons, whereas the low-frequency crossing characterizes the heavy plasmons,[6]

$$\tilde{\omega}_p^* = \left[ 6 \left[ 1 + \frac{n_f}{n_c} \right] \right]^{1/2} T^* , \tag{1}$$

where $T^*$ is the renormalized Fermi temperature (usually identified with $T_K$), and $n = n_c + n_f$ is the total carrier density, relevant to low-frequency electrodynamics.[2] The heavy-fermion plasma mode reflects not only the heavy quasiparticle mass ($m^*/m_b$), but also the renormalized Coulomb screening.[2]

At very low frequencies, the heavy-fermion conductivity is phenomenologically described by the following (renormalized Drude) expression:

$$\sigma(\omega) = \frac{ne^2\tau^*}{m^*} \frac{1}{1 - i\omega\tau^*} , \tag{2}$$

where $m^*$ and $\tau^*$ are the renormalized mass and relaxation time of the quasiparticles, respectively. From Eq. (2) one can then define a so-called renormalized plasma frequency (or unscreened heavy plasmon)

$$\omega_p^* = \left[ \frac{4\pi n e^2}{m^*} \right]^{1/2} \tag{3}$$

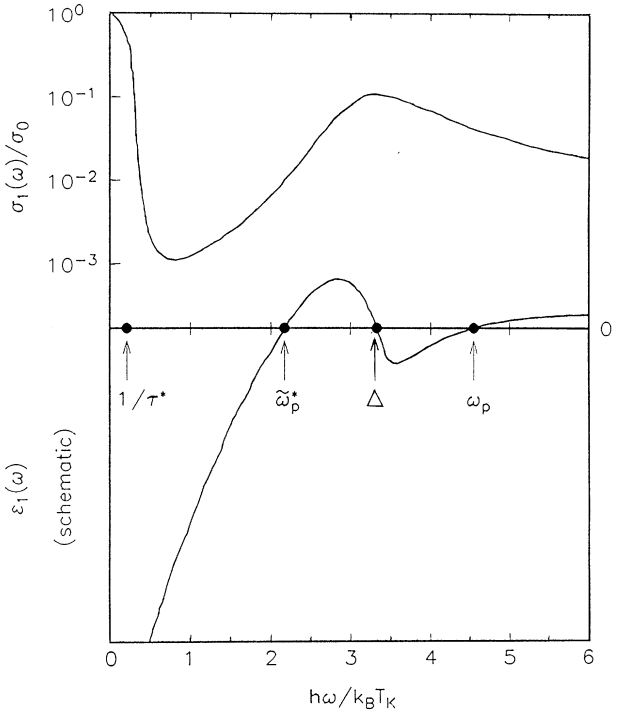


FIG. 1. The calculated dynamical conductivity for heavy fermions (see, for example, Ref. 3). The lower zero crossing at $\tilde{\omega}_p^*$ of the dielectric function $\varepsilon_1(\omega)$ implies a heavy-plasma mode.

0163-1829/93/48(15)/10692(9)/$06.00

which is experimentally obtained as the spectral weight of the narrow resonance in the electrodynamic response, centered at $\omega=0$ and extending up to the minimum in $\sigma_1$, near $h\nu \sim k_B T_K$. In normal metals, with a simple Drude response, $\omega_p^*$ is also the frequency where the dielectric constant crosses over from negative to positive value. Here, also because of a high-frequency response, the zero crossing frequency is different and corresponds to $\tilde{\omega}_p^*$, defined in Eq. (1). $\tilde{\omega}_p^*$ can be alternatively written in the form $\tilde{\omega}_p^* = (m_b/m^*)^{1/2}\Delta$ and basically corresponds to the so-called screened renormalized plasma frequency.

Irrespective of the particular model, the general spectral weight considerations imply the following relation between the two plasma frequencies (i.e., $\omega_p^*$ and $\omega_p$),

$$\left[\frac{\omega_p}{\omega_p^*}\right] = \left[\frac{m^*}{m_b}\frac{n_c}{n}\right]^{1/2}, \tag{4}$$

so that a measurement of $\sigma(\omega)$ over a broad frequency range allows an ideal evaluation of the enhanced effective mass in the heavy-fermion ground state.[8]

Two different experimental techniques have been employed to explore the low-temperature electrodynamics in several heavy fermions. Optical measurements have clearly established a narrow resonance in materials such as $CePd_3$, $UPt_3$, and $CeCu_6$.[9–12] However, these results are somewhat uncertain due to the high reflectivity of the heavy-fermion materials at low frequencies. This leads to some controversies, e.g., about an unambiguous detection of the onset of the broad background, as well as the minimum in $\sigma_1$, at frequencies near $k_B T_K$.[9,11,12] On the other hand, surface impedance experiments,[8] while, in principle, more sensitive at low frequencies than the optical methods, have been plagued by difficulties which arise when measuring both components of the surface impedance $Z_s = R_s - iX_s$, i.e., the surface resistance $R_s$ and the surface reactance $X_s$. These issues have been addressed recently,[13] and the question of whether the optical or the surface impedance results are more reliable has not been resolved.

In this paper we review our experiments involving both the surface impedance and the optical measurement on $CeAl_3$, a prototype example of the heavy-fermion compounds. Its dc resistivity $\rho_{dc}$, shown in the inset of Fig. 2(a), displays a peak around $T_{max} \sim 35$ K, below which the many-body correlations become important. In transport terminology, therefore, $T_{max}$ represents the onset of coherence effects which are responsible for the marked decrease in $\rho_{dc}$ with sample cooling. Below $T_{max}$ a heavy-fermion system is in the so-called Kondo-lattice regime, whereas at higher temperatures the many-body correlations are suppressed by thermal fluctuations and the local moments act as incoherent scattering centers, characteristic of the single Kondo-impurity regime. Both the susceptibility $\chi$ and the specific-heat coefficient $\gamma$ are enhanced at low temperatures and below 300 mK, $\rho_{dc} = AT^2$, with a large coefficient[14] $A = 35\ \mu\Omega\,\mathrm{cm\,K^{-2}}$. These parameters are consistent with an enhanced effective mass of the quasiparticle. Furthermore, at liquid-He temperature, both $\chi$ and $\gamma$ are temperature dependent, suggesting strongly temperature-dependent renormalization effects.

It is generally agreed[1–6] that the temperature-dependent enhancement of $\gamma$ and $\chi$ is a consequence of the gradual buildup of many-body correlations at the Fermi level, giving rise to a many-body (Abrikosov-Suhl-Kondo) resonance of width $k_B T_K$ in the density of states. Regarding the electrodynamics of correlated systems, one expects the many-body and normal-state regimes to be well separated at low temperatures, with a narrow resonance in the conductivity at low frequencies, and the normal metallic behavior recovered at high energies. This is expected to be particularly evident in $CeAl_3$ as suggested by the large enhancements of its thermodynamic properties.[15] As we will see, our experimental results do show this characteristic behavior.

In our experiments the absorptivity was obtained over a broad spectral range by combining the microwave and far-infrared (FIR) data. Kramers-Kronig (KK) analysis was subsequently performed in order to completely evaluate the frequency-dependent conductivity $\sigma(\omega) = \sigma_1(\omega) + i\sigma_2(\omega)$. At microwave frequencies, we have also evaluated both parts of the complex conductivity directly from $R_s$ and $X_s$. Within experimental accuracy, the two methods were found to give the same frequency-dependent complex conductivity at various temperatures. From our $\sigma(\omega)$ data we extract the frequency- and

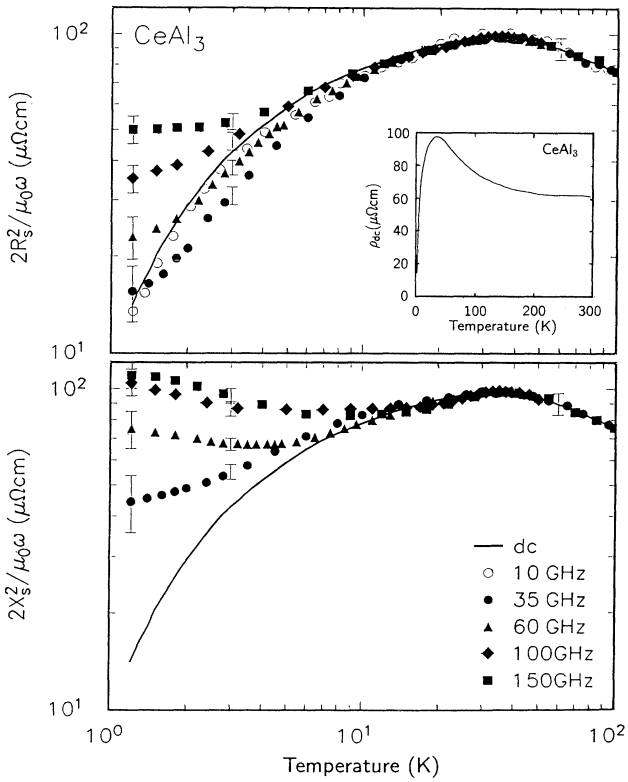


FIG. 2. Temperature dependence of the complex surface impedance, and the dc resistivity of $CeAl_3$. The choice of the particular representations of $R_s$ and $X_s$ is made to show the frequency-independent behavior at high temperatures.

temperature-dependent optical scattering rate and the mass enhancement. We compare the temperature dependence of the effective mass obtained from the dynamical conductivity, with thermodynamic quantities. Finally, we discuss the universality of enhancements in the optical and thermodynamic properties of various materials where electron-electron interactions are of importance.

This paper is organized as follows. In Sec. II we describe our measurements and present the results. A detailed discussion of our findings follows in Sec. III and, finally, the conclusions are stated in Sec. IV.

## II. EXPERIMENT AND RESULTS

The polycrystalline samples used for our investigations were produced by combining the stoichiometric amounts of starting materials using an arc furnace. Wrapped in Ta foil and sealed in quartz tubes under a pressure of 150 Torr of Ar, they were then annealed for 10 days at 800 °C. The high-purity and single-phase nature of our specimens were subsequently demonstrated by the x-ray analysis. The samples were cut using a spark cutter and polished with 1-$\mu$m liquid-based Alumina abrasive before any measurements were performed.

Measurements of the surface impedance[8] ($Z_s = R_s - iX_s$) were accomplished by polishing a planar surface of the sample and then clamping it at the bottoms of cylindrical copper cavities so as to form their end plates. The width ($\Gamma_0$) and frequency ($f_0$) of the cavity resonance are altered when its copper end plate is replaced by the sample. These changes (at each temperature) are related to the sample's surface resistance $R_s$ and reactance $X_s$, respectively, as follows:[8]

$$R_s - R_s^{\mathrm{Cu}} = k\Delta\Gamma_0 , \tag{5a}$$

$$X_s - X_s^{\mathrm{Cu}} = -2k\Delta f_0 + X_0 , \tag{5b}$$

where ($R_s^{\mathrm{Cu}} - iX_s^{\mathrm{Cu}}$) is the surface impedance of copper, $k$ reflects the resonator constant for the cavity end plate and the geometry of the specimen, and $X_0$ is a temperature-independent constant, depending on the end-plate mounting.

To be able to evaluate $R_s$ and $X_s$, both $k$ and $X_0$ have to be known. We have assumed that at $T > 30$ K $CeAl_3$ is in the so-called Hagen-Rubens limit $\omega\tau \ll 1$. In this limit, $\sigma_1 \gg \sigma_2$ and $R_s = X_s = (-i\mu_0\omega\sigma_1^{-1})^{1/2}$. The measured dc resistivity $\rho_{\mathrm{dc}} = 1/\sigma_1$ then gives a calculated $R_s$, which together with $\Delta\Gamma_0$, gives, from Eq. 5(a), $k$. Then, $k$, the calculated $X_s$, and the measured $\Delta f_0$ give, through Eq. (5b), $X_0$.[16,17]

By exciting the cavities in the $TE_{011}$ mode,[8] both components of $Z_s$ were obtained as functions of temperature at 35, 60, 100, and 150 GHz. At 10 GHz only the surface resistance was measured employing a cavity perturbation technique.[18] It consists of introducing a small sample in a resonant cavity, and measuring the change in its resonance characteristics. We chose the size of the sample to be small compared to the spatial variation of the fields so as not to perturb the cavity mode. Further details of the surface impedance measurements techniques are described in Refs. 8, 16, and 18.

The reflectance measurements were performed on polished samples from the same batch, within six months of the surface impedance measurements. In the 15–700-$cm^{-1}$ range a Bruker IFS 113$v$ fast-Fourier-transform interferometer was used, followed by a fast-scanning Bruker interferometer (IFS 48PC) for the 600–5000-$cm^{-1}$ frequency region. The data over the 4500–32 000-$cm^{-1}$ range were obtained with a homemade spectrometer based on a Zeiss monochromator and, finally, the high-frequency region of 28 000–96 000 $cm^{-1}$ was covered with a McPherson spectrometer. A freshly evaporated gold mirror served as a reference for all measurements below 5000 $cm^{-1}$. For the 15–400-$cm^{-1}$ region we employed a Hg arc source and a $He_{4.2}$-cooled ($He_{1.2}$ cooled below 100 $cm^{-1}$) silicon bolometer. In the 400–5000-$cm^{-1}$ range a globar source and a deuterated triglycerine sulfate (DTS) detector were used. Above 5000 $cm^{-1}$ these were replaced by a tungsten lamp and an InSb photodetector. Over 4500–32 000 $cm^{-1}$ we utilized a tungsten halogen lamp for the source and a phototube for the detector.

The reflectivity data from different source-detector combinations showed a mismatch of at most 3% in their absolute values. The spectra in the individual ranges were then joined at overlapping frequencies by multiplying with constant correction factors. The measurements were repeated after a year on different samples from the same batch, and the reflectivity was reproducible to within 0.5%, 1%, 3%, and 5% over the spectral ranges below 700, 700–5000, 4000–32 000, and above 30 000 $cm^{-1}$, respectively. With this well-accepted variation in the reflectance data, we are confident that the effects of a possible oxide-layer formation on the surface of the samples are minimal on our measurements.

Figure 2 shows the measured micrometer- and millimeter-wave frequencies. The dc resistivity displayed in the inset was measured before and after all the optical and surface impedance measurements were performed. Its absolute value was reproducible within 2%. The surface impedance measurements were performed as a function of temperature from 1.2 to 300 K. At low temperatures, the frequency-dependent increase of the resistivity ($2R_s^2/\mu_0\omega$) results from a steady loss of coherence, due to the ac perturbation. In the normal skin-depth regime, the surface impedance and the complex conductivity (the dynamical response function) are related as

$$Z_s = R_s - iX_s = \left[\frac{-i\mu_0\omega}{\sigma_1 + i\sigma_2}\right]^{1/2} . \tag{6}$$

In the high-temperature range the scattering rate ($1/\tau$) is significantly larger than the millimeter-wave frequencies, and $\sigma_2$ is negligible compared to $\sigma_1$. Consequently the following approximations of Eq. (6) (the so-called Hagen-Rubens limit) are valid at these temperatures:

$$Z_s = \left[\frac{-i\mu_0\omega}{\sigma_{\mathrm{dc}}}\right]^{1/2} , \tag{7a}$$

$$\frac{R_s}{Z_0} = \frac{X_s}{Z_0} = \left[\frac{\varepsilon_0\omega\rho_{\mathrm{dc}}}{2}\right]^{1/2} , \tag{7b}$$

where $\rho_{dc}$ is the dc resistivity and $Z_0=377\ \Omega$ is the free-space impedance. We utilize this fact in the analysis of our surface impedance data as follows.

Above $T_{max}\sim 35$ K the temperature dependences of $R_s$ and $X_s$ at millimeter-wave frequencies were found to be the same within experimental uncertainty (error bar in Fig. 2), suggesting a frequency-independent response at high temperatures. At $T_{max}$, the absolute values of $2R_s^2/\mu_0\omega$ in different runs were within a factor of 2 of the corresponding dc resistivity. The variation results from different samples and/or nonuniformity of a sample's surface characteristics. Furthermore, due to a somewhat broad resistivity maximum, the data near $T_{max}$ are least susceptible to any thermal gradients in the cavity and/or fluctuations of its characteristics. The data were therefore normalized at this temperature to remove the arbitrariness in the absolute value of $Z_s$. This arbitrariness results from the sample-surface irregularities and from the fact that $X_s$ can be measured only up to a temperature-independent constant $X_0$, since the effective size of the cavity depends on the sample-mounting details.[16,17]

The end-plate mounting was repeatable to within 4 $\mu$m, as inferred from the frequency reproducibility of the cavities with repeated mountings, to within 0.05–0.2 %. The constant $X_0$ was determined by taking the real and imaginary parts of the surface impedance equal in the high-temperature range, where their temperature dependences were found to be the same. Notice that the error bar at high temperatures reflects the maximum margin of uncertainty in the data normalization, as well as the deviations from a perfect Hagen-Rubens behavior [Eq. (7b)]. The uncertainty in the surface impedance takes into account the scatter of the data in individual runs, due mostly to the fluctuations in the microwave source output, and the thermal stresses in the cavity. Although the actual uncertainty in $R_s$ is slightly smaller than that in $X_s$, we report the larger of the two for the worst-case error estimates.

For the purpose of the KK analysis we first combined the microwave and optical measurements in order to obtain the absorptivity over a broad spectral range. The absorptivity and surface impedance are related according to (Ref. 16, p. 80)

$$A=\frac{4R_s}{Z_0}\frac{1}{1+2R_s/Z_0+(R_s^2+X_s^2)/Z_0^2}\ . \tag{8}$$

The last two terms in this expression are negligible compared to the first term since $R_s, X_s \ll Z_0$ in the submillimeter to microwave spectral range, for a highly conducting material such as $CeAl_3$. Combining these results together with $A=1-R$, where $R$ is the optical reflectance from 15 to $10^5$ cm$^{-1}$, we obtain the absorptivity from microwave frequencies up to 12 eV, as shown in Fig. 3. The absolute absorptivity at 15 cm$^{-1}$ was normalized to the 10-K Hagen-Rubens value. The $\pm 15\%$ error in the absorptivity at 15-cm$^{-1}$ results from a 0.5% uncertainty of the reflectivity over the FIR spectral range. Since we were unable to experimentally cover the spectral region between 5 and 15 cm$^{-1}$, we linearly interpolated our data (broken line in Fig. 3) in this narrow region before performing the KK analysis. This interpolation as well as those between the surface impedance data were obtained by spline curve fitting.

Above 15 cm$^{-1}$ the absorptivity spectrum does not show any temperature dependences. Results at microwave frequencies show, however, a strong frequency and temperature dependence below approximately 10 K (Fig. 3). By 10 GHz the measured absorptivity is close to the Hagen-Rubens (HR) extrapolation [Eq. (7b), dots in Fig. 3] within our measurement sensitivity. To show the detailed temperature variation of the absorptivity, we have plotted in Fig. 3(b) a close-up of $A$ in the 0.1–10-cm$^{-1}$ range. The error bars in the surface impedance data reflect the uncertainties in $R_s$ at 1.2 K, whereas at higher temperatures, the symbol size itself is a measure of the uncertainty.

In Fig. 4 we show the real part of the optical conductivity $\sigma(\omega)=\sigma_1(\omega)+i\sigma_2(\omega)$ and in Fig. 5 the real part of the dielectric function $\varepsilon_1(\omega)=1-\sigma_2(\omega)/\varepsilon_0\omega$ is shown, as obtained from the KK analysis of the data in Fig. 3. We have found that, in spite of the nonlocal nature of the Kramers-Kronig transformation, the uncertainty in our absorptivity data [Fig. 3(b)] produces a local $\pm 20\%$ (i.e.,

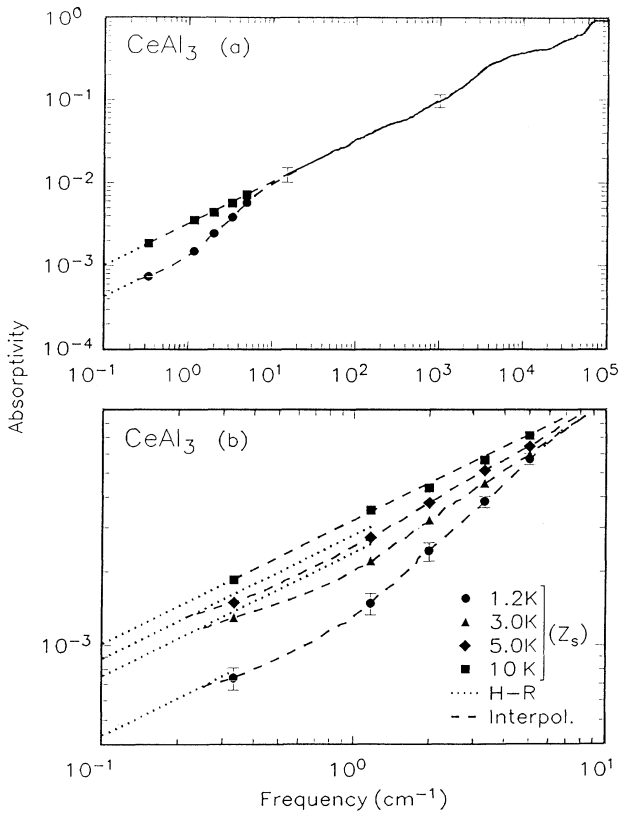


FIG. 3. (a) Frequency dependence of the absorptivity $A=1-R$ of $CeAl_3$ at 1.2 and 10 K. Both optical and microwave data are displayed in the figure. (b) Temperature-variation of $A$ in the 0.1–10-cm$^{-1}$ range. Notice the (measurable) dip in the absorptivity below the Hagen-Rubens line at 3 K.

an uncertainty at the same frequency) uncertainty in $\sigma_1(\omega)$ and $\pm 25\%$ in $\varepsilon_1(\omega)$. To obtain both components of the complex conductivity at millimeter-wave frequencies, we make use of Eq. (6). Before applying this relationship we must first qualify the electronic response in our material as appropriate to the classical skin effect, i.e., the normal skin depth ($\delta_{cl}$) is larger than the carrier mean free path ($l$). Neglecting a weak dependence on the carrier density in metals ($n^{2/3}$), the ratio $\delta_{cl}/l$ can be related to that for copper at the same frequency as follows (Ref. 16, p. 76):

$$\left[\frac{\delta_{cl}}{l}\right]^{\text{test}} = \left[\frac{\delta_{cl}}{l}\right]^{\text{Cu}} \left[\frac{\rho_{dc}(\text{test})}{\rho_{dc}(\text{Cu})}\right]^{3/2} . \quad (9)$$

For conservative estimate, using $\rho_{dc}(CeAl_3) = 14\ \mu\Omega$ cm at 1.2 K, and the fact that $\rho_{dc}(Cu) = 1.7\ \mu\Omega$ cm at 300 K, we infer that at least for frequencies up to which copper (at room temperature) is in the classical skin-depth regime, so is our test specimen $CeAl_3$. This certainly holds up to our highest millimeter-wave frequency of measurement, i.e., 150 GHz (see, e.g., Ref 19, p. 93). Consequently, we use the measured $R_s$ and $X_s$ values (shown in Fig. 2) and Eq. (6) to obtain both components of the conductivity at millimeter-wave frequencies. Thus, $\sigma_1$ and $\varepsilon_1$ obtained directly from $R_s$ and $X_s$ are also displayed in Figs. 4 and 5. The uncertainty in the $Z_s$ data ($\pm 10\%$ in $R_s$ and $X_s$) corresponds to a maximum of $\pm 23\%$ in $\sigma(\omega)$, calculated at the millimeter-wave frequencies.

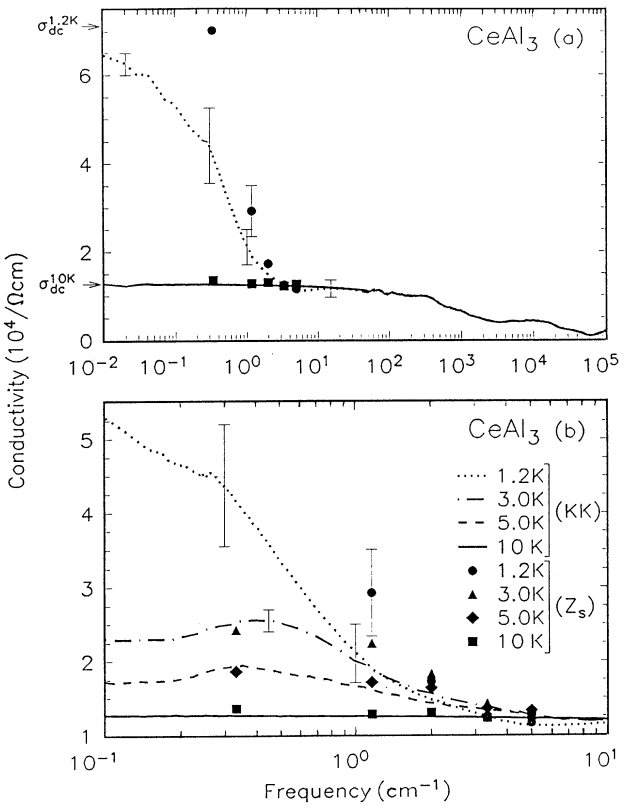


FIG. 4. (a) Frequency-dependent conductivity obtained from the Kramers-Kronig analysis of the data in Fig. 3, and directly from the surface impedance measurements. (b) a close-up of the dynamical conductivity showing the development of the low-frequency resonance at low temperatures. The 10-GHz point from the surface resistance data is equal to $(2R_s^2/\mu_0\omega)^{-1}$ (see text).

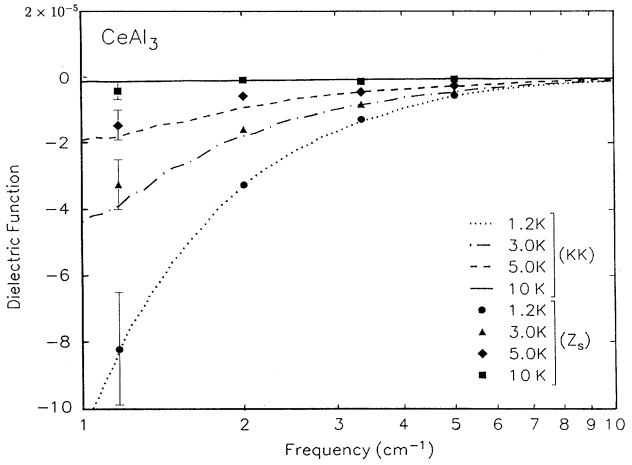


FIG. 5. Frequency dependence of the dielectric function at four temperatures, with an excellent agreement between the Kramers-Kronig values, and those evaluated from the surface impedance data.

We qualify that the 10-GHz point [equal to $(2R_s^2/\mu_0\omega)^{-1}$] represents an upper bound on the conductivity evaluated from the surface resistance data (assuming $R_s = X_s$), rather than an exact value. This point is shown only to provide an estimate of the maximum possible discrepancy that can be expected between the conductivity obtained from the two methods. In the absence of the $X_s$ data an appropriate uncertainty estimate cannot be made at this frequency. For a realistic comparison of the two methods, we therefore confine our attention to 35–150-GHz range.

Within experimental accuracy both methods give the same frequency-dependent $\sigma_1(\omega)$ and $\varepsilon_1(\omega)$ at different temperatures, and consequently we believe that the signatures of the observed frequency-dependent response are free of experimental ambiguities, which were discussed earlier.[13] However, we must emphasize that while $\sigma_1$ at 1.2 K obtained by the KK transformation has developed some frequency dependence by 0.3 $cm^{-1}$, our cavity-perturbation data at the same frequency of 10 GHz follows the dc resistivity [see Fig. 2(a)]. Furthermore, we notice that the conductivity evaluated from the KK analysis is lower than that obtained from the surface impedance measurements both at the millimeter-wave frequencies, as well as when $\omega \to 0$. These differences, we believe, are due to the uncertainties of the evaluation of $\sigma_1$ and $\sigma_2$ using the two different methods. These, however, do not affect our conclusions, as will be discussed later.

## III. DISCUSSION

First of all, we remark that the optical conductivity at 10 K (and above) is suggestive of a frequency-

independent behavior with a relaxation rate $1/(2\pi\tau)\sim 800$ cm$^{-1}$. However, the agreement between the extrapolation of $\sigma_1$ for $\omega\rightarrow 0$, obtained from the KK analysis, and $\sigma_{dc}$ is excellent. In contrast, below 10 K we observe the gradual emergence of a narrow resonance in $\sigma_1$, and the low-temperature results join the 10-K conductivity at about 3 cm$^{-1}$. Here, $\sigma_1(\omega\rightarrow 0)$ from the KK analysis and $\sigma_{dc}$ at 1.2 K match within 10%. The most interesting feature in $\sigma_1(\omega)$, as the sample temperature is lowered below 10 K, is the rapid buildup of the low-frequency spectral weight [Fig. 4(b)], manifesting a gradual emergence of the many-body effects. Below we discuss some of the unusual features of $\sigma(\omega)$ in the low-temperature, coherent state.

As mentioned before, even though the conductivity at 1.2 K has acquired a frequency dependence below 0.3 cm$^{-1}$, the absorptivity displays a Hagen-Rubens–type behavior. This anomaly may be understood as follows. As expected from the free-carrier electrodynamic response, beyond a frequency defined by the (enhanced) relaxation time, the low-temperature absorptivity should become frequency independent in the so-called relaxation regime, even as the conductivity continues to drop below its dc value. However in $CeAl_3$, a crossover from the coherent to the normal metallic behavior starts before this regime is entered, as manifested by the frequency dependence in the scattering rate (see later in this section). This (opposing) factor tends to increase the absorptivity towards its unrenormalized value that characterizes the high-temperature response, and thus keeps it close to the Hagen-Rubens line.

The overall behavior of the frequency-dependent conductivity at low temperatures is, in general, similar to that obtained in various calculations.[1,20,21] Nevertheless, the expected minimum in $\sigma_1$ at $h\nu\sim k_B T_k$ is not resolved in the excitation spectrum down to 1.2 K. Similar results have been reported for HF compounds $UPt_3$ and $CePd_3$ as well, by Sulewski *et al.* and Webb, Sievers, and Mihalisin.[9,10] However, Marabelli and co-workers observed this minimum for $CeCu_6$ and $UPt_3$.[11,12] Therefore, the universality of this feature is a matter of debate.[9,11,12] We tend to believe that at temperatures comparable to or only slightly below the Kondo temperature, the system is in the so-called overdamped regime and consequently, the thermal broadening screens out the heavy plasma mode associated with a $\sigma_1$ minimum.

In Fig. 4(b) we notice at 3 and 5 K a small anomaly in $\sigma_1$ at about 1 cm$^{-1}$. This is due to the fact that the microwave absorptivity at these temperatures is slightly lower than the HR value [Fig. 3(b)], while the relaxation regime [characterized by $\sigma_2(\omega)\geq\sigma_1(\omega)$] is not yet entered. This dip exceeds the uncertainty margin in the absorptivity at 3 K [symbol size in Fig 3(b)] and therefore, we believe it to be a real effect. Since in the Drude metallic response, the saturation of the absorptivity beyond the relaxation edge is accompanied by a monotonic fall off of $\sigma_1$, our results at 3 K may suggest a small deviation from the dominant, free-carrier behavior.

As far as the dielectric function $\varepsilon_1(\omega)$ is concerned (Fig. 5), the low-frequency results from the Kramers-Kronig analysis and from surface impedance measurements are in excellent agreement. In the UV region the dielectric function is found to cross zero at about $6\times 10^4$ cm$^{-1}$. In the absence of interband transitions this would be the optical plasma frequency $\omega_p$. We will return to this point later in the discussion. Various theoretical treatments of the heavy-fermion electrodynamics predict additionally a heavy plasma mode [Fig. 1, Eq. (1)],[2,6] which may be observable as a second, low-frequency zero crossing of the dielectric function at temperatures $T\ll T_K$, as mentioned in the introduction. Bredl *et al.*[22] have estimated a $T_K=3$ K for $CeAl_3$. Thus, the HF plasma mode is expected at $\tilde{\omega}_p^*\sim 5.1$ cm$^{-1}$. We see no clear-cut evidence in our experimental results of such a low-frequency zero crossing in $\varepsilon_1(\omega)$ (and therefore, of $\tilde{\omega}_p^*$) down to 1.2 K $<T_K$ (Fig. 5). Evidently, the heavy plasmon mode is too overdamped at 1.2 K, and may only be observable well below liquid-$^3$He temperatures.

In order to show the detailed temperature dependence of $\sigma_1$ and $\varepsilon_1$, we have plotted these quantities obtained from the surface impedance measurements, as functions of temperature in Fig. 6. Consistent with the observation of Fig. 2, no frequency dependence is seen above $\sim 10$ K, while at lower temperatures a strongly temperature-dependent carrier scattering gives rise to peaks in the microwave conductivity. Of course, at high temperatures the absence of any frequency dependence implies

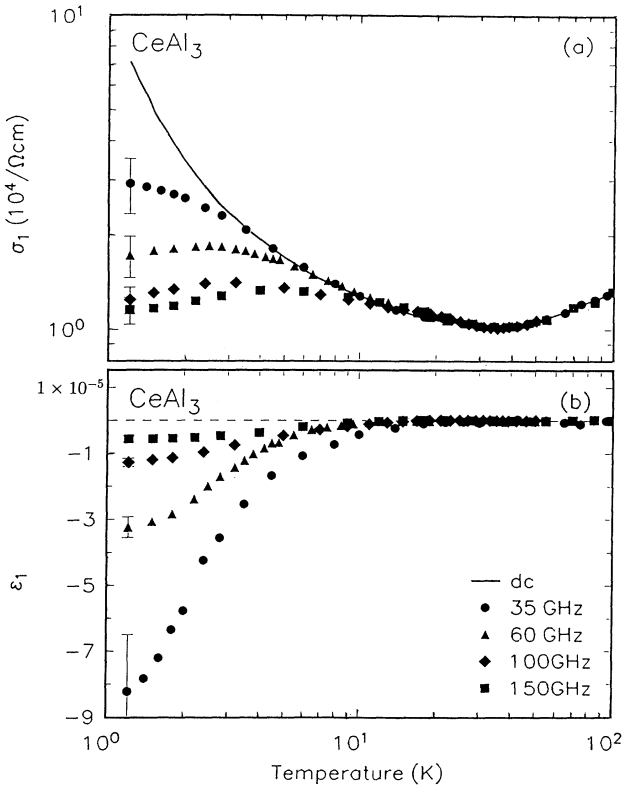


FIG. 6. Temperature dependence of $\sigma_{dc}$ and $\sigma_1$ (a), and of $\varepsilon_1$ (b) at millimeter-wave frequencies, evaluated from the surface impedance data. The high-temperature behavior is expectedly frequency independent, whereas the low-temperature maxima in $\sigma_1$ are due to a strongly temperature-dependent scattering rate.

$\sigma_2 \ll \sigma_1$, and therefore the dielectric function at various frequencies approaches 1 [Fig. 6(b)].

To characterize the many-body renormalizations, we make use of the (model-independent) sum-rule argument: the ratio of the spectral weight associated with the low-lying resonance to that of the high-temperature, frequency-independent response is of the order of $m_b/m^*$ [c.f., Eq. (4)], where $m_b$ is the band mass and $m^*$ is the effective quasiparticle mass.[1] These spectral weights are obtained by evaluating the following integrals of our $\sigma_1(\omega)$ data [Fig. 4(a)]:

$$I_1 = \int_0^{\omega_c} \sigma_1(\omega, 1.2\ \mathrm{K})\, d\omega = \frac{\pi n e^2}{2m^*} = \frac{(\omega_p^*)^2}{8} , \tag{10a}$$

$$I_2 = \int_0^{\omega_h} \sigma_1(\omega, 10\ \mathrm{K})\, d\omega = \frac{\pi n e^2}{2m_b} = \frac{\omega_p^2}{8} , \tag{10b}$$

where $\omega_c \sim 3\ \mathrm{cm}^{-1}$, the frequency above which the conductivity at 10 K is indistinguishable (within our experimental error), from that at lower temperatures, and $\omega_h$ is (roughly) the frequency above which the interband processes dominate $\sigma_1$.

At 10 K, above a frequency of $\sim 2500\ \mathrm{cm}^{-1}$ where the conductivity has dropped below half its dc value and is starting to flatten again, its free-carrier part was taken to roll off as $\omega^{-2}$. From the spectral weight of the free-carrier response at 10 K we thus determine the unscreened optical plasma frequency for $CeAl_3$ to be $h\nu_p = 3.5$ eV. This frequency is clearly smaller than the zero-crossing frequency (7.5 eV) of the dielectric function, implying the strong influence of the interband transitions. These transitions, if at frequencies $> \omega_p$, tend to lower the $\varepsilon_1$ zero-crossing frequency, due to their screening effect. On the other hand, the transitions at frequencies $< \omega_p$ would tend to push the zero crossing towards higher frequencies. This reversal of role of an interband transition at $\omega_{ib}$ (say) happens because of its capacitive screening of the electromagnetic fields for $\omega < \omega_{ib}$ (i.e., $\sigma_2^{ib} < 0$), while for $\omega > \omega_{ib}$ its shielding effect is inductive ($\sigma_2^{ib} > 0$) (see, e.g., Ref. 19, p. 46). Our results then suggest the predominance of the low-frequency (i.e., at $\omega_{ib} < \omega_p$) interband transitions. From Fig. 4(a) we notice at least one such structure, at about $10^4\ \mathrm{cm}^{-1}$ ($\sim 1$ eV $< h\nu_p$).

The ratio $I_2/I_1$ now gives $m^*/m_b = 325 \pm 50$ at 1.2 K. The uncertainty in $m^*$ corresponds to that of $\pm 20\%$ in the Kramers-Kronig conductivity (Fig. 4), evaluated by taking into account the uncertainties in the surface impedance and the FIR reflectivity data (Fig. 3). This approach, however, is not suitable to estimate the temperature dependence of $m^*$, since the low-frequency resonance becomes increasingly less distinguishable from the frequency-independent response at high-temperatures, making it harder to estimate the ratio $I_2/I_1$.

Another method of estimating $m^*/m_b$ together with the scattering rate $\Gamma$ is to consider the low-frequency resonance arising from free carriers undergoing frequency-dependent scattering so that the complex conductivity may be written as[9,23]

$$\sigma(\omega) = \frac{\omega_p^2/4\pi}{\Gamma(\omega) - i\omega(m^*/m_b)} , \tag{11}$$

where $\omega_p$ is the unscreened optical plasma frequency. To be exact, this representation for $\sigma(\omega)$ is appropriate at $T = 0$ K. At finite temperatures we use this as an operational definition of $\Gamma(\omega)$ and $m^*(\omega)$. A relationship between $\sigma_1$, $\sigma_2$, and $\Gamma$ together with $m^*/m_b$ is then obtained as follows:

$$\Gamma(\omega) = \frac{\omega_p^2}{4\pi} \frac{\sigma_1}{|\sigma|^2} , \tag{12a}$$

$$\frac{m^*(\omega)}{m_b} = \frac{\omega_p^2}{4\pi} \frac{\sigma_2}{\omega |\sigma|^2} . \tag{12b}$$

When $\omega \ll \Gamma$ and $\omega \to 0$, $\sigma_1$ is constant and $\sigma_2$ should tend to zero, while both $\Gamma(\omega)$ and $m^*(\omega)$ must assume frequency-independent values.

We first discuss the frequency-dependent scattering rate $\Gamma(\omega, T)$, shown in Fig. 7(a) at several temperatures. For this purpose, the value of $h\nu = 3.5$ eV, obtained from the spectral weight consideration of the 10-K data, was used [$I_2$ in Eq. (10b)]. At frequencies $\omega = 2\pi\nu$, for which $h\nu \ll k_B T$, the scattering rate is primarily determined by the temperature. With this expectation, the curves in Fig. 7(a) have been terminated at 0.2 $\mathrm{cm}^{-1}$ (1.2 K $= 0.8$

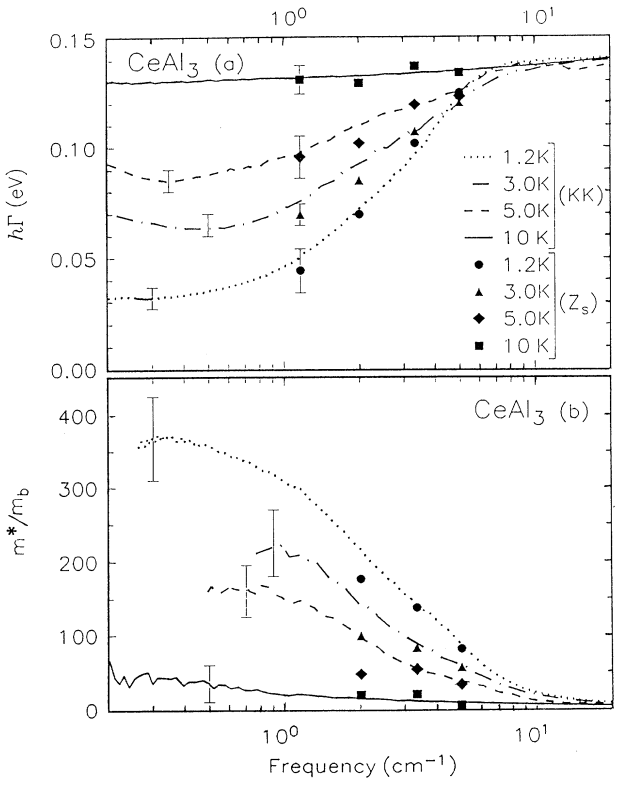


FIG. 7. Frequency-dependent optical scattering rate (a) at four temperatures from Eq. (12a), along with the values obtained using the microwave data. (b) Frequency dependence of $m^*$ obtained from Eq. (12b). Below the low-frequency cut off, the effective-mass values are artifactual (see text).

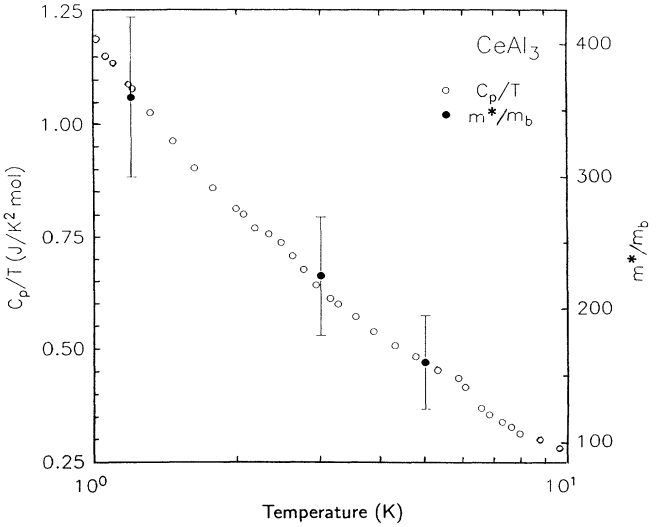


FIG. 8. Temperature dependence of the effective dynamical mass obtained from Fig. 7(b). Also shown for comparison is $C_p/T$ (Ref. 24).

$cm^{-1}$). Also shown are the values obtained directly from the surface impedance measurements using Eqs. (6) and (12a), which are in excellent agreement with those from the KK analysis. At each temperature, the error bar on the 35-GHz point also represents the maximum percentage uncertainty in the higher-frequency surface impedance results. Above approximately 7 $cm^{-1}$, the temperature dependence of $\Gamma$ disappears, while at low frequencies, the scattering rate is only temperature dependent, thus eliminating the need for uncertain extrapolations. The latter simplification is possible because of the measurements extending down to very low frequencies. Interestingly, by 10 K ($=7$ $cm^{-1}$), there is little frequency dependence left in $\Gamma$ as well. Over the range showing the strong frequency dependence of $\Gamma$, a simple Drude picture with constant parameters does not apply. Moreover, while the frequency dependence of $\sigma_1$ is due to a small scattering rate, its rolloff to a finite value starts where $\Gamma$ acquires a significant frequency dependence.

The previous analysis also gives the frequency-dependent effective mass, as shown in Fig. 7(b). At 10 K and above, the coherent state does not exist as the surface impedance results suggest (Fig. 2), and consequently no mass enhancement is expected. Indeed in Fig. 7(b), the 10-K data scatter (between 10 and 50) is within the uncertainty in the effective mass. We expect $m^*$ in Eq. (11) to assume constant values at frequencies below which $\Gamma$ becomes frequency independent. This crossover frequency [say $\omega_{co}(T)$] is approximately 0.3, 0.9, and 0.7 $cm^{-1}$ at 1.2, 3.0, and 5.0 K, respectively [Fig. 7(a)]. Although the scattering rate saturates below the $\omega_{co}$'s, we obtained a continued frequency dependence of the low-temperature effective mass. Since small deviations of the reflectivity from a perfect analytic function affect the imaginary part of the KK conductivity much more than its real part, then from Eq. (12b), $\sigma_2(\omega)$ can give rise to a spurious frequency dependence of $m^*$. In light of this possibility, the unexpected behavior of $m^*$ at low frequencies [not shown in Fig. 7(b)] is to be considered an artifact. The values of $m^*/m_b$ at the $\omega_{co}$'s are 360, 225, and 160, which we believe to be appropriate estimates of the zero-frequency effective masses at these temperatures. Thus, a substantial increase in the effective mass occurs only below 3 K (for $CeAl_3$, $T_K \sim 3$ K!).

Furthermore, we can now remark that the frequency dependence of $\sigma_1$ below $\omega_{co}$ is determined by an effective scattering rate. Defining the latter as $\Gamma_{eff}=[\Gamma(m_b/m^*)]$ at $\omega_{co}$, its values are 0.7, 2.5, and 4.5 $cm^{-1}$ at 1.2, 3, and 5 K, respectively. It is worth noting that these values agree with the width of the narrow resonance in the optical conductivity [Fig. 4(b)]. These values exceed the $\omega_{co}(T)$'s, supporting the previously discussed interpretation of an anomalous Hagen-Rubens behavior, observed at low temperatures in our microwave data. The frequency dependence of $\Gamma$ is strongest where the electromagnetic response of the system crosses over from one characteristic (i.e., highly renormalized) behavior at low frequencies, to the normal metallic kind at high frequencies. One of the implications is the loss of frequency dependence of $\sigma_1$ over the same range, as seen in Fig. 4. Moreover, the $T$- and $\omega$-dependent contributions to $\Gamma(\omega)$ seem to be of comparable magnitudes in Fig. 7(a).

Finally, in Fig. 8 we show the effective mass vs temperature, along with the specific-heat ($C_p/T$) data.[24] The two sets of results were normalized (somewhat arbitrarily) at 5 K for the purpose of comparison. The low- and high-temperature saturation limits of the electrodynamical mass are associated with the narrow resonance in the

TABLE I. A summary of the optical and thermodynamic parameters of four heavy-fermion compounds.

| Compound | $h\nu_p$ (eV) | $h\nu_p^*$ (eV) | $m^*/m_b$ | $\gamma(0)$ ($J/K^2$ mol) | $m^*/m_e$ |
|---|---|---|---|---|---|
| $CeAl_3$ | 3.5[a] | 0.194[a] | 325 | 1.62[e] | 690 |
| $CeCu_6$ | 1.8[b] | 0.150[b] | 150 | 1.30[f] | 600 |
| $CePd_3$ | 2.3[c] | 0.350[c] | 40 | 0.04[g] | 44 |
| $UPt_3$ | 2.6[d] | 0.323[d] | 65 | 0.42[f] | 240 |

[a]Present work.
[b]Reference 12.
[c]Reference 10.
[d]Reference 9.
[e]Reference 14.
[f]Reference 15.
[g]Reference 25.

density of states (DOS), and the broad underlying band, respectively. At mid temperatures, the effective dynamical mass has intermediate values due to a temperature-dependent Fermi-surface renormalization. Regarding the thermodynamic experiments, $C_p/T$ and $\chi$ primarily measure the DOS at the Fermi level (averaged over an energy width $k_B T$). The decrease of $C_p/T$ and $\chi$ with temperature reflects the gradual disappearance of correlation effects, and the contribution of higher-order temperature corrections. For $T \sim T_K$, the many-body resonance width, these higher-order terms (in the Bethe-Sommerfeld expansion) become important. Consequently, $C_p/T$ may not be expected to give the correct temperature dependence of the effective mass directly. Nevertheless, it is remarkable that the thermodynamic and electrodynamic quantities have comparably similar temperature dependences (Fig. 8). Precisely what can be learned from this peculiar correspondence remains to be seen.

## IV. CONCLUSION

In this paper, we have examined the frequency-dependent conductivity of the extremely correlated heavy-fermion compound $CeAl_3$. At low temperatures, we observe a zero-frequency resonance in the dynamic conductivity. The frequency and temperature dependence of the scattering rate and the effective mass were evaluated and compared with thermodynamic measurements. We suggest that the narrow resonance is due to correlation effects. This conclusion is based on the observed temperature-dependent effective mass, and the crossover behavior of the scattering rate with frequency, which cannot be obtained from a multiband picture. An analysis involving several bands[9] has been found to be inadequate. We find that the analysis of thermodynamics and electrodynamics leads to similar effects, both expressed in terms of a renormalized effective mass. This feature is general, and applies to various strongly correlated metallic systems. In order to give a summary of the renormalization effects for heavy fermions, we show in Table I the two plasma frequencies $\omega_p$ and $\omega_p^*$, and the resultant mass enhancement $m^*/m_b$ for four well-studied compounds. Also shown in the same table are the low-temperature limiting value of the specific-heat coefficient $\gamma(0)$, and the enhancement over the free-electron mass, obtained by combining[8] $\omega_p^*$ and $\gamma(0)$. The renormalizations of the plasma frequency and of the specific-heat coefficient are evidently consistent with the enhancement of the quasiparticle mass.

## ACKNOWLEDGMENTS

We acknowledge S. Donovan for his help with the 10-GHz measurements. We have also benefited from many fruitful discussions with P. Fulde, K. Becker, A. J. Millis, P. Wachter, and T. M. Rice. One of us (L.D.) wishes to acknowledge financial support from the Swiss National Science Foundation. This research was supported by NSF grants at UCLA and UCSD.

*Present address: L. Boltzmann Institut, Kopernikusgasse 15, A-1060 Vienna, Austria.

†Present address: Laboratorium für Festkörperphysik der ETH-Zürich, CH-8093 Zürich, Switzerland.

[1] A. J. Millis and P. A. Lee, Phys. Rev. B **35**, 3394 (1987).

[2] A. J. Millis, M. Lavagna, and P. A. Lee, Phys. Rev. B **36**, 864 (1987).

[3] P. Coleman, Phys. Rev. Lett. **59**, 1026 (1987).

[4] K. W. Becker and P. Fulde, Z. Phys. B **67**, 35 (1987).

[5] W. Brenig and K. W. Becker, J. Magn. Magn. Mater. **76&77**, 252 (1988).

[6] P. Fulde, J. Keller, and G. Zwicknagl, in *Solid State Physics: Theory of Heavy-Fermion Systems,* edited by H. Ehrenreich and D. Turnbull (Academic, New York, 1988), Vol. 41, p. 1.

[7] R. Freytag and J. Keller, Z. Phys. B **80**, 241 (1990).

[8] A. M. Awasthi, W. P. Beyermann, J. P. Carini, and G. Grüner, Phys. Rev. B **39**, 2377 (1989).

[9] P. E. Sulewski, A. J. Sievers, M. B. Maple, M. S. Torikachvili, J. L. Smith, and Z. Fisk, Phys. Rev. B **38**, 5338 (1988).

[10] B. C. Webb, A. J. Sievers, and T. Mihalisin, Phys. Rev. Lett. **57**, 1951 (1986).

[11] F. Marabelli, G. Travaglini, P. Wachter, and J. J. M. Franse, Solid State Commun. **59**, 381 (1986).

[12] F. Marabelli and P. Wachter, Phys. Rev. B **42**, 3307 (1990).

[13] P. E. Sulewski and A. J. Sievers, Phys. Rev. Lett. **63**, 2000 (1989); W. P. Beyermann and G. Grüner, *ibid.* **63**, 2001 (1989).

[14] K. Andres, J. E. Graebner, and H. R. Ott, Phys. Rev. Lett. **35**, 1779 (1975).

[15] G. R. Steward, Rev. Mod. Phys. **56**, 755 (1984).

[16] A. M. Awasthi, Ph.D. thesis, University of California at Los Angeles, 1991.

[17] For an undercoupled resonator, the intrinsic losses predominate over those due to its coupling to the transmission lines.

[18] L. I. Buranov and I. F. Shchegolev, Prib. Tekh. Eksp. **2**, 171 (1971).

[19] F. Wooten, *Optical Properties of Solids* (Academic, New York, 1972).

[20] N. Grewe and T. Pruschke, Z. Phys. B **60**, 311 (1985).

[21] D. L. Cox and N. Grewe, Z. Phys. B **71**, 321 (1988).

[22] C. D. Bredl, S. Horn, F. Steglich, B. Lüthi, and R. M. Martin, Phys. Rev. Lett. **52**, 1982 (1984).

[23] G. Thomas, J. Orenstein, D. H. Rapkine, M. Capizzi, A. J. Millis, R. N. Bhatt, L. F. Schneemeyer, and J. W. Waszczak, Phys. Rev. Lett. **61**, 1313 (1988).

[24] G. E. Brodale, R. A. Fisher, and N. E. Phillips, Phys. Rev. Lett. **56**, 390 (1986).

[25] J. M. Lawrence, R. S. Risenborough, and R. D. Parks, Rep. Prog. Phys. **44**, 1 (1981).